Small-Angle X-ray Scattering Reveals an Extended Organization for the Autoinhibitory Resting State of the p47^{phox} Modular Protein

Dominique Durand,*,§ Dominique Cannella,‡ Virginie Dubosclard,‡ Eva Pebay-Peyroula,‡ Patrice Vachette,§ and Franck Fieschi*,‡

IBBMC, CNRS UMR8619 Université Paris Sud, Bât. 430, 91405 Orsay Cedex, France, and Institut de Biologie Structurale, UMR 5075 CEA/CNRS/Université Joseph Fourier, Laboratoire des Protéines membranaires, 41 rue Jules Horowitz 38027 Grenoble Cedex 1, France

Received February 8, 2006; Revised Manuscript Received April 20, 2006

ABSTRACT: In response to microbial infection, neutrophiles promote the assembly of the NADPH oxidase complex in order to produce superoxide anions. This reaction is activated by the association of cytosolic factors, p47^{phox}, p67^{phox}, p40^{phox}, and a small G protein Rac with the membranous heterodimeric flavocytochrome b_{558}, composed of gp91^{phox} and p22^{phox}. In the activation process, p47^{phox} plays a central role as the target of phosphorylations and as a scaffolding protein conducting the translocation and assembly of cytosolic factors onto the membranous components. The PX and tandem SH3s of p47^{phox} have been highlighted as being key determinants for the interaction with membrane lipids and the p22^{phox} component, respectively. In the resting state, the two corresponding interfaces are thought to be masked allowing its cytoplasmic localization. However, the resting state modular organization of p47^{phox} and its autoinhibition mode are still not fully understood despite available structural information on separate modules. More precisely, it raises the question of the mutual arrangement of the PX domain and the tandem SH3 domains in the resting state. To address this question, we have engaged a study of the entire p47^{phox} molecule in solution using small-angle X-ray scattering. Despite internal autoinhibitory interactions, p47^{phox} adopts an extended conformation. First insights about the domain arrangement in whole p47^{phox} can be derived. Our data allow to discard the usual representation of a globular and compact autoinhibited resting state.

The NADPH oxidase of neutrophil is a multicomponent enzyme essential in innate immunity as exemplified by a genetic disorder, chronic granulomatous disease (CGD),[1] in which NADPH oxidase activity is impaired. This enzyme represents one of the best defense lines against microbial infection through its ability to catalyze oxygen reduction to superoxide as a first step toward a global reactive oxygen species production called the oxidative burst (*1*). This highly destructive power is at the origin of a number of diseases when inappropriately activated. Thus, a tight regulation of this membranous enzyme is required. NADPH oxidase is composed of a membrane-integrated flavocytochrome b_{558} (gp91^{phox} and p22^{phox}), which constitutes the catalytic core of the enzyme, and of three cytosolic factors (the modular proteins p47^{phox}, p67^{phox}, and p40^{phox}), as well as a small G protein, Rac.

In the resting state, components involved in an active NADPH oxidase complex are physically separated. Indeed, they are partitioned in different subcellular locations. Activation requires the translocation of the cytosolic factors and of the Rac protein to the membrane and their assembly with the flavocytochrome b_{558} to constitute a fully active NADPH oxidase complex. The cytosolic factors are modular proteins containing various domains allowing protein−protein or lipid−protein interactions (*2*−*4*). The molecular events occurring during translocation and assembly of the oxidase involve a complex set of interactions mediated by these protein modules. Upon exposure to specific stimuli, activation is initiated through multiple phosphorylation events on the cytosolic components. Among them, p47^{phox} plays a central role in the assembly process. From the N- to the C-terminus, p47^{phox} comprises a PX domain, a tandem of SH3 domains, a polybasic region involved in autoinhibition (Auto Inhibitory Region) and a polyproline motif toward the C-terminal end (Figure 1A). p47^{phox} can be considered as the sensor of the activation signal through multiple phosphorylations (*5*−*9*). In CGD patients lacking p47^{phox}, no translocation of the p67^{phox} and p40^{phox} factors to the membrane takes place (*10*, *11*). Thus, in addition to its "activation sensing" role, p47^{phox} is a scaffolding protein conducting translocation and assembly of the other cytosolic factors to the membrane component of the oxidase. Indeed, in its activated state, p47^{phox} is able to interact with phosphatidyl inositol lipids of the plasma membrane through its PX domain (*12*, *13*) and with the C-terminal polyproline motif of the p22^{phox} subunit through its tandem of SH3

* Corresponding authors. F. Fieschi: phone, +33 4 38789177; fax, +33 4 38785494; e-mail, fieschi@ibs.fr. D. Durand: phone, +33 1 69156421; fax, +33 1 69853715; e-mail, dominique.durand@ibbmc.u-psud.fr.

‡ Université Paris Sud.

§ Université Joseph Fourier.

[1] Abbreviations:PX, Phox homology; SH3, src homology 3; CGD, chronic granulomatous disease; AIR, autoinhibitory region; NMR, nuclear magnetic resonance; SAXS, small-angle X-ray scattering; GST, glutathione *S*-transferase; IPTG, iso-propyl β-D-thiogalactopyranoside; DR, dummy residue; PDB, Protein Data Bank.

10.1021/bi060274k CCC: $33.50
Published on Web 05/20/2006

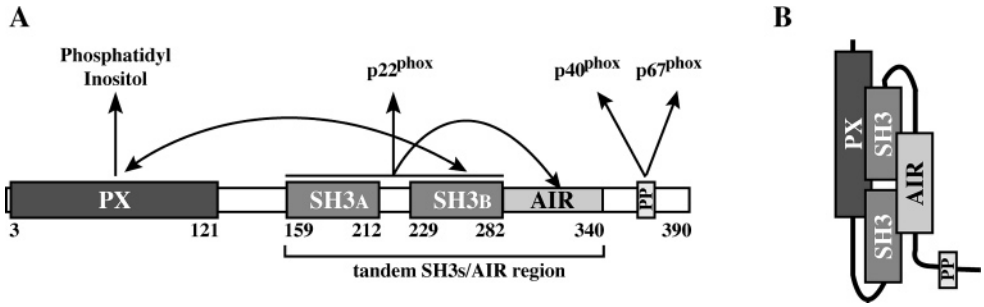

FIGURE 1: Schematic representations of p47^{phox}, a cytosolic factor of the NADPH oxidase complex. (A) Domain organization in p47^{phox}, arrows indicate all interactions that have been shown experimentally (*12*, *14*, *15*, *24*, *58*−*63*). (B) Proposed model for the domain organization in the autoinhibitory state of p47^{phox} (*4*, *20*, *21*, *64*, *65*).

domains (Figure 1A) (*14*−*17*). In the fully assembled complex, additional interactions, still poorly characterized, have been reported between p47^{phox} and gp91^{phox} (*18*, *19*). However, the PX- and tandem SH3s-mediated interactions have been pinpointed as being the key determinants initiating translocation to the membrane and docking the p40^{phox}−p67^{phox}−p47^{phox} cytosolic complex onto the flavocytochrome b_{558} (*20*, *21*). In the resting state, p47^{phox} is unable to promote these two interactions. Numerous biochemical and, more recently, structural studies argue for the existence of an autoinhibitory mechanism in the resting state in which binding sites on both the PX domain and the tandem SH3s are masked and thereby unavailable for interaction with their respective ligands, phosphatidyl inositol and p22^{phox} polyproline motif (*13*, *16*, *20*−*22*). It has been shown that phosphorylation of C-terminal serines of p47^{phox}, and more precisely of Ser 303, 304, and 328, are necessary to activate the binding properties toward phosphatidyl inositol and p22^{phox} polyproline motif, thereby allowing activation and assembly of the whole NADPH complex to proceed (*8*, *13*, *20*).

The autoinhibitory state of p47^{phox} and its mechanism of release have been the subject of detailed molecular studies. However, these various data have been interpreted in terms of conflicting models for the autoinhibited p47^{phox} state, so that to date no global model accounts for all p47^{phox} properties. A first model for the regulation of the lipid binding properties of PX domain through the resting and the activated states was based on the presence of a consensus PxxP motif between α2 and α3 helices of this domain. This feature suggested a possible interaction with an SH3 domain masking the lipid binding site (Figure 1) (*13*). Such an interaction between PX and the second SH3 domain of p47^{phox} (SH3$_B$) has been observed and characterized by NMR using isolated domains (*23*). Moreover, W263R mutation in the polyproline binding site of SH3$_B$ has been shown to restore the phosphatidyl inositol phosphate binding capability of entire p47^{phox} in a manner similar to the effect of C-terminal serine phosphorylation (*13*). These observations led to the proposal that lipid-binding inhibition results from an intramolecular interaction between PX and the SH3$_B$ domain.

A second model accounts for the autoinhibition of the interaction of the p47^{phox} SH3 domains with p22^{phox}. Fine and accurate biochemical studies have established the role of the polybasic region downstream from the SH3$_B$ domain (residues 296−340) through simultaneous interactions with both SH3$_A$ and SH3$_B$ (*14*, *20*, *24*). This model for inhibition has been strongly supported by the structure of the p47^{phox} region encompassing residues 156−340, containing the two SH3 domains and the AIR/polybasic region (*16*, *25*). This structure is based on the crystal structure of an intertwined dimer of p47^{phox} (156−340) and shows that the AIR folds back, in an unusual manner, into a groove formed by the two SH3 domains interface. Therefore, the release of the AIR following phosphorylation can be easily explained by steric and electrostatic effects. Finally, combination of NMR and SAXS data confirmed this structural autoinhibition of the SH3 tandem by the AIR in this p47^{phox} (156−340) truncated form (*26*) in solution.

These two autoinhibitory mechanisms relying on intramolecular interactions have led to a widely accepted and extensively presented model of the p47^{phox} autoinhibitory resting state organization as depicted in Figure 1B. However, both the PX domain inhibition and the p22^{phox} interaction inhibition exhibit some mutual incompatabilities from a structural and a functional standpoint as already pointed out in a recent review (*4*). Both require the same interaction site with the SH3$_B$ domain as a key element in the locking system. This suggests that, in the context of the entire p47^{phox} protein, the relations between the various domains are more complicated than now depicted. More precisely, it raises the question of the actual autoinhibitory interactions within the whole molecule and, in particular, that of the mutual arrangement of the PX domain and the tandem SH3 domains. Further progress in our knowledge of the autoinhibitory state of p47^{phox} will not result from structural studies restricted to isolated domains. However, three-dimensional crystallographic structures of multidomain proteins such as p47^{phox} are difficult to reach due to their modular and flexible character. We have therefore initiated a structural study of the entire p47^{phox} in solution using small-angle X-ray scattering (SAXS). We present here the first insights about the domain architecture of the whole p47^{phox} in its autoinhibited state.

EXPERIMENTAL PROCEDURES

p47^{phox} Expression and Purification. The p47^{phox} protein is expressed as a GST fusion protein using a pGex-6P-derived vector containing the p47^{phox} cDNA sequence. This vector has been kindly provided by M. C. Dagher. The protein was expressed in *Escherichia coli* BL21(DE3) strain. Expression is induced with 0.5 mM IPTG, when cell culture reached an OD of 0.6 at 600 nm. After overnight induction at 20 °C, cells were harvested and resuspended in chilled lysis buffer (50 mM Tris, pH 7, 0.3 M NaCl, 1 mM EDTA,

and 2 mM DTT). All following operations were carried out at 4 °C. Cells were disrupted by sonication, then centrifuged at 40 000 rpm for 40 min in a Beckman 45 Ti rotor. The supernatant was loaded onto a 4 mL Gluthation-Sepharose 4B column (Amersham) equilibrated in the previous buffer. Proteins were eluted at 1 mL/min with 50 mL of elution buffer (50 mM Tris, pH 8, 0.1 M NaCl, and 10 mM Glutathion). Fractions containing GST-p47^{phox} were pooled and subjected to a 4 h digestion at 4 °C with 2.2 units Prescission protease per mg of protein (Amersham). Due to the genetic construction, digested p47^{phox} possesses 10 and 7 additional residues at its N- and C-terminus, respectively. Digestion products were loaded at a flow rate of 0,5 mL/min onto a MonoS column (Amersham) equilibrated in 50 mM Hepes, pH 8, 50 mM NaCl, 1 mM EDTA, and 2 mM DTT. The proteins were eluted with a 40 mL linear gradient of NaCl (50−500 mM). The resulting protein fractions containing p47^{phox} were concentrated, on a centrifugal concentration device with a 30 kDa cutoff, to 300 μL and diluted in 4 mL of Hepes 50 mM pH 8, 100 mM NaCl, 1 mM EDTA, 2 mM DTT, and 5% glycerol. The proteins were finally re-concentrated and, at different concentrations, aliquots of p47^{phox} were taken and stored for SAXS experiments.

SAXS Measurements and Data Analysis. Scattering data were recorded on the small-angle X-ray scattering instrument D24 at LURE (Laboratoire pour l'Utilisation du Rayonnement Electromagnétique, Orsay, France) using the radiation emitted by a bending magnet of the storage ring DCI. The wavelength λ was selected by a bent Ge(111) monochromator and adjusted to 1.488 Å, calibrated by the nickel absorption edge. X-ray patterns were recorded using a linear position-sensitive detector with delay-line readout. The sample-to-detector distance was 1378 mm corresponding to the scattering vector range: $0.013\ \text{Å}^{-1} < Q < 0.34\ \text{Å}^{-1}$ (where $Q = 4\pi \sin\theta/\lambda$, 2θ is the scattering angle). The sample was placed in a quartz capillary, the temperature of which was kept constant ($T = 4$ °C) via a water circulation. Air and window scattering was virtually eliminated by inserting the cell in an evacuated beam path (*27*). Several successive frames (usually eight) of 200 s each were recorded for both the sample and the corresponding buffer. Each frame was carefully inspected to check for any protein damage induced by X-rays (none was found) before calculating the average intensity and the associated experimental error. Each scattering spectrum was corrected for the detector response and scaled to the transmitted intensity, using the scattering intensity from a reference carbon-black sample integrated over a given angular range. The scattering from the buffer was measured and subtracted from the corresponding protein sample pattern.

Scattering patterns were recorded at four different protein concentrations from 1 to 6.5 mg/mL. After scaling for concentration, the smallest angle data exhibited a slight increase with concentration indicative of moderate attractive interactions between molecules. Data were extrapolated to zero concentration following standard procedures using the second virial coefficient (*28*) (see inset to Figure 2A). The scattering from a 5 mg/mL solution of lysozyme in 50 mM acetate buffer, pH 4.5, and 100 mM NaCl was recorded and used as a calibration sample to derive the molecular mass from the intensity at the origin. The radius of gyration R_g was first evaluated using the Guinier approximation (*29*), using data points out to $Q_{max}R_g = 1.25$. Restricting Q_{max} down to $Q_{max}R_g = 0.88$ left the R_g value unchanged. The R_g value was also derived from the distance distribution function $p(r)$ that represents the histogram of distances within the particle. Its value is equal to zero when r exceeds D_{max}, the maximum dimension of the protein. The $p(r)$ function was computed using the indirect transform package GNOM (*30*). To ensure that no significant amount of oligomers nor even residual attractive concentration effects were affecting the data, a series of $p(r)$ calculations was performed in which an increasing number of the smallest angle data points were eliminated reaching $Q = 0.04\ \text{Å}^{-1}$, thereby excluding the entire Guinier region. No significant effect was detected in the resulting $p(r)$ functions nor in the R_g value.

Modeling. The conformation in solution of p47^{phox} was determined using three approaches. The program DAMMIN represents the protein as an assembly of closely packed small spheres (dummy atoms) of radius $r_0 \ll D_{max}$ inside a sphere of diameter D_{max} (*31*). The DAM structure is defined by a configuration vector $\mathbf{X}$ with $N \approx (D_{max}/r_0)^3$ components; $X(i) = 1$ if the ith dummy atom belongs to the protein and $X(i) = 0$ otherwise. Using simulated annealing, the program searches for a configuration that fits the experimental data, while a looseness penalty ensures the compactness and connectivity of the solution. No particular condition of particle shape was imposed as constraint in these calculations.

The program GASBOR uses a protein representation as a chain of dummy residues (DR) centered at the Cα positions (*32*). Starting from a gaslike distribution of DRs inside the same search volume as DAMMIN, the program condenses this distribution so as to fit the experimental data under constraints that ensure the chainlike character of the DRs spatial distribution. Thus, each elementary step moves a DR to a new location 0.38 nm from another randomly chosen DR. Furthermore, the penalty function imposes a protein-like distribution of nearest neighbors and minimizes the number of discontinuities along the chain, while maintaining the center of mass close to the center of the search volume. The program was run in default mode using standard values of the parameters. It was also used with a reduced weight of the penalty term ensuring that the nearest neighbor distribution would resemble that of a compact protein.

Like all Monte Carlo approaches, neither DAMMIN nor GASBOR yields a unique solution. Therefore, several (typically 10) low-resolution models are constructed using each program before being superimposed using the program DAMAVER which calculates the normalized spatial discrepancy (NSD) between all pairs of models (*33*). This allows one, after elimination of outliers, to select the most typical model defined as the model with the smallest NSDs to all other models, that is, that is most similar to other models.

Finally, the program BUNCH implements a combination of *ab initio* and rigid body modeling using the high-resolution structures of rigid domains of the protein when available (*34*). It finds the optimal positions and orientations of domains and probable conformations of flexible linkers represented as DR chains that are attached to the appropriate end of domains. The scattering amplitudes of rigid domains are first calculated using the program CRYSOL (*35*). The scattering pattern is calculated using partial amplitudes of domains together with form factors of DRs describing the loops. To

take into account the contribution to scattering of hydration water around DRs, the scattering amplitude of each DR was multiplied by a factor of 1.2, a value derived from a rough estimate of the average amount of hydration water. The scattering pattern of the final model was calculated using CRYSOL and found to be practically undistinguishable from the BUNCH result, while differences were observed in the absence of correction (factor = 1.0), showing that this simple improvement was both necessary and effective.

RESULTS

The scattering pattern after correction for interparticle effects is shown in Figure 2A (dots), while the inset displays a close-up view of the affected part of the curve (see Experimental Procedures for details). The corresponding distance distribution function $p(r)$ is shown in Figure 2B (dots). The value of the maximal diameter of the molecule was found to be 125 ± 5 Å. The values of the radius of gyration derived from Guinier's law and the $p(r)$ function are 34.0 ± 0.5 and 34.7 ± 0.2 Å, respectively. Using lysozyme as a reference sample and taking into account the presence of 5% glycerol in the p47^{phox} solution, we found the molecular mass for p47^{phox} derived from the intensity at the origin to be close to 50 kDa, in agreement with the known molecular mass derived from the primary sequence (46 365 Da), thereby ruling out any significant aggregation and showing that the protein is monomeric.

Both D_{max} and R_g values are considerably larger than those expected for a compact globular protein with the molecular mass of p47^{phox} which are of the order of 70−80 and 22−24 Å, respectively. This shows that the protein adopts an elongated conformation in solution. This is also strongly suggested by the $p(r)$ function that exhibits a peak around 25 Å and a long falling edge extending to large r values, an asymmetric profile typical of an elongated particle.

Two *ab initio* modeling approaches implemented in DAMMIN and GASBOR programs were used to determine the shape of p47^{phox} from scattering intensities out to Q_{max} = 0.25 and 0.34 Å^{-1}, respectively. Ten low-resolution models were constructed using each program before being superimposed using the program DAMAVER so as to determine the most typical model. The results from both approaches are very similar: all resulting models are elongated, most of them getting thinner at one end. All calculated scattering patterns are in excellent agreement with experimental data ($\chi \sim 0.9$). A few Dummy Residue (DR) models obtained using GASBOR are presented in Figure 3A.

In a second modeling stage, protein domains whose structures had been determined by crystallography or NMR are positioned within the most typical low-resolution model. We have used the best representative conformer out of the 20 models of the PX domain determined by NMR (pdb file 1GD5 (*23*); rms deviation from average coordinates of about 1 Å over all non-hydrogen atoms). Regarding the pair of SH3 domains, we assumed that their conformation within intact p47^{phox} is close to that determined in the crystal for the truncated protein (157−332) comprising neither the PX domain nor the linker between this domain and the SH3$_A$ domain nor the C-terminal part, a conformation in which the SH3 tandem interacts with a polybasic region called the autoinhibitory region (AIR) (*20*). Within the crystal, this truncated molecule is present as a dimer having swapped part of their SH3$_A$ domain (*16*, *25*). Starting from the dimer structure (pdb file: 1ng2.pdb (*16*)) we have built a conformation of the monomer tandem-SH3s/AIR by restoring the exchanged fragment. These domains of known structure were positioned within the most typical low-resolution model using the superimposition program SUPCOMB while imposing a distance restraint between the C-terminal end of the PX domain and the N-terminal end of the tandem-SH3s/AIR rigid domain (Figure 3B).

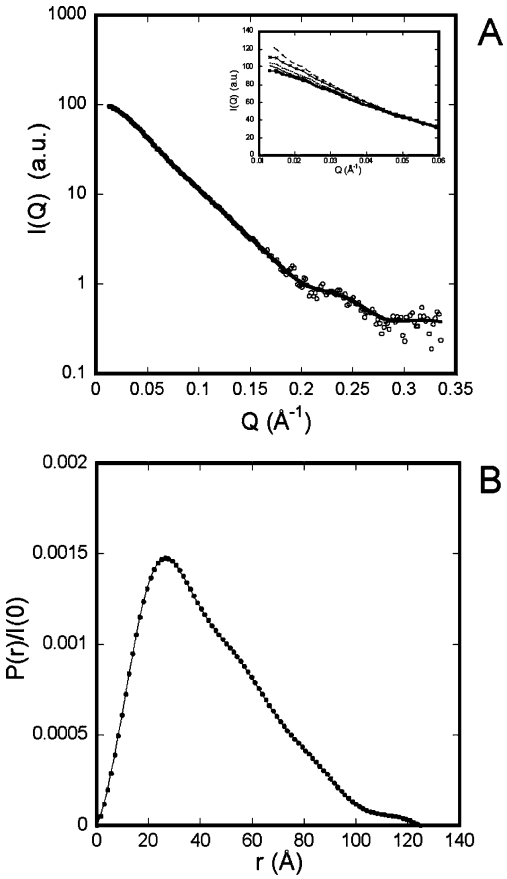

FIGURE 2: (A) SAXS pattern of p47^{phox} after correction for interparticle effects. Dots, experimental points; solid line, fit to the data by the BUNCH model shown in Figure 3C. Inset: Experimental intensities in the smallest-angle region as a function of protein concentration (long-dashed line, 6.5 mg/mL; continuous line with x, 4 mg/mL; short-dashed line, 2 mg/mL; thin continuous line, 1 mg/mL; thick continuous line, intensities extrapolated to infinite dilution). (B) Distance distribution function $p(r)$.

In a last step of the modeling process, the three missing parts are modeled as DR chains: the first 10 N-terminal residues, the 28 residue-long linker between PX and N-SH3 domains, and the C-terminal part comprising 65 residues. This was performed using the program BUNCH. The PX domain and the tandem-SH3s/AIR domain were fixed at their initial position determined in the previous step. The resulting configurations compatible with this constraint exhibit a linker exposed to the solvent while remaining in the vicinity of the domains. The C-terminal stretch is always in an external position, away from the two domains. It appears to be poorly structured with no defined shape, and its compactness, though variable, is lower than that of a structured domain. The corresponding calculated scattering patterns agree well with experimental data ($\chi \sim 0.85$ with randomly distributed residuals, see Figure 2). Two typical models are shown in

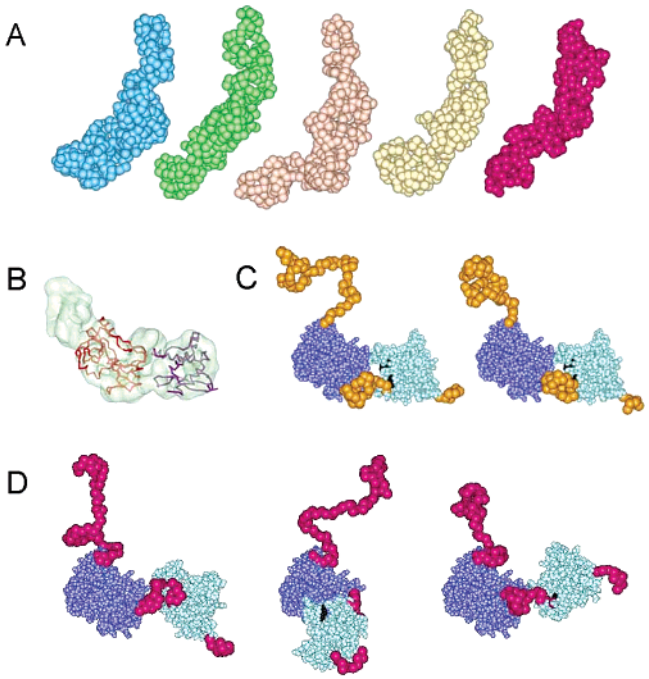

FIGURE 3: (A) Five models of p47^{phox} obtained using GASBOR (see text for details). (B) Crystal structures of PX and SH3 tandem fitted in the GASBOR model using SUPCOMB. The crystal structures are represented by their Cα trace (violet, PX; red, tandem SH3s/AIR). The model is represented by its surface envelope in transparent light green. (C) Two examples of p47^{phox} conformations obtained using BUNCH with the two partial crystal structures (CPK representation) maintained at the fixed position derived from SUPCOMB (lavender, SH3 tandem; cyan, PX). The *ab initio* models of the unknown linker and extremities are shown as orange spheres of radius 3.2 Å (see text for details). (D) Three examples of p47^{phox} conformations obtained using BUNCH in which the mutual position of the two partial crystal structures was refined by the program. The SH3 tandem is in the same position as in panel C. The ab initio models of the unknown linker and extremities are shown as magenta spheres of radius 3.2 Å. In Figure 4C,D, Arg45 and 92 are shown in black when at all visible. All figures have been made using the program WebLab ViewerLite 40 (Molecular Simulation Inc.).

Figure 3C. In this figure, each DR is represented by a sphere of radius 3.2 Å whose volume is equal to the average volume of an amino acid residue, that is, about 140 Å^3. Since the distance between two adjacent DRs is 3.8 Å (see Experimental Procedures), neighboring spheres are overlapping. Models were also calculated while releasing the constraint and leaving both domains free to move with respect to one another. In the resulting configurations, the two domains are not in contact any more but remain close with a closest distance of ca. 5 Å, and the intervening linker is rather compact, but the orientation of the PX domain can vary widely as can be seen in the three models displayed in Figure 3D. The agreement between the calculated scattering pattern and the experimental data is equally good ($\chi \sim 0.83$). The values of R_g and D_{max} of all models displayed in Figure 3C,D are the same as those derived from experimental data within experimental uncertainty.

DISCUSSION

Our results show that in the unphosphorylated, autoinhibited state, isolated p47^{phox} adopts an elongated conformation in solution. The values of both the radius of gyration and the maximal diameter as well as ab initio models are unambiguous. The two structured domains (PX and the SH3 tandem/AIR domains) cannot form a globular assembly. We tried to simulate the experimental scattering curve starting from a conformation in which PX and the tandem SH3 form such a compact globule. All these attempts failed, yielding χ values ≥ 3. Therefore, the protection of PX phosphoinositol lipid binding sites necessary to the maintenance of the resting state does not involve a compact arrangement of domains. Many diagrams, admittedly with no claim to structural value, summarizing the various interactions within p47^{phox} and the changes following phosphorylation show a transition from a "close", compact, conformation in the resting state to an "open" conformation in the activated state (see Figure 1B and references therein). It follows from our results that "open" and "close" must be considered more in a functional than a structural sense. Besides, some of the proposed interactions appear to be mutually incompatible as mentioned earlier.

Both structured domains can easily be accommodated within the ab initio elongated envelope from Gasbor, thereby providing a starting point for modeling missing parts using BUNCH. This was done keeping the two structured domains fixed in their starting position or letting the program refine their position and orientation.

The various resulting conformations exhibit common features.

(i) The C-terminal part, comprising 65 residues, does not adopt a well-defined structure, the chain being more or less compact, but it is always pointing away from the two structured domains. To somewhat quantify this description, we can compare the dimensions of the C-terminal part with those of a globular domain and with those of a chain with persistence length that is the adequate description for an unfolded polypeptide chain (*36*). Assuming for such a chain a persistence length of the order of 9−10 Å, a value commonly found in the literature (*37*), the end-to-end distance is of the order of 60 Å for a 65 residue-long chain. The conformations found within our models exhibit shorter end-to-end distances, between 30 and 55 Å, which could be compatible with the presence of some structure in the C-terminal region. In contrast, the D_{max} value of the C-terminal part is comprised between 45 and 75 Å, larger than the value of around 30 Å expected for a 65-residue compact globular domain. The C-terminal extremity therefore appears to be mainly unstructured but not completely unfolded. We have examined the amino acid sequence of the C-terminal 107 residues using several programs predicting unfolded segments (*38*−*45*). The results are very similar and summarized in Figure 4A: all programs predict the 65 C-terminal residues to be essentially disordered with, for three of them, the exception of the very last stretch. Programs predicting secondary structure elements (*46*−*49*) predict a unique helix formation for the very last residues. Interestingly enough, this helix has been experimentally observed when the C-terminal 30 residues from p47^{phox} are complexed with the C-terminal SH3 domain from p67^{phox} (*50*). The body of computational or experimental evidence presented above broadly agrees with a description of the C-terminal 65 residues in terms of a mostly unfolded chain with a few local structure elements. Finally, the fact that the C-terminal part is always pointing away from the two structured domains

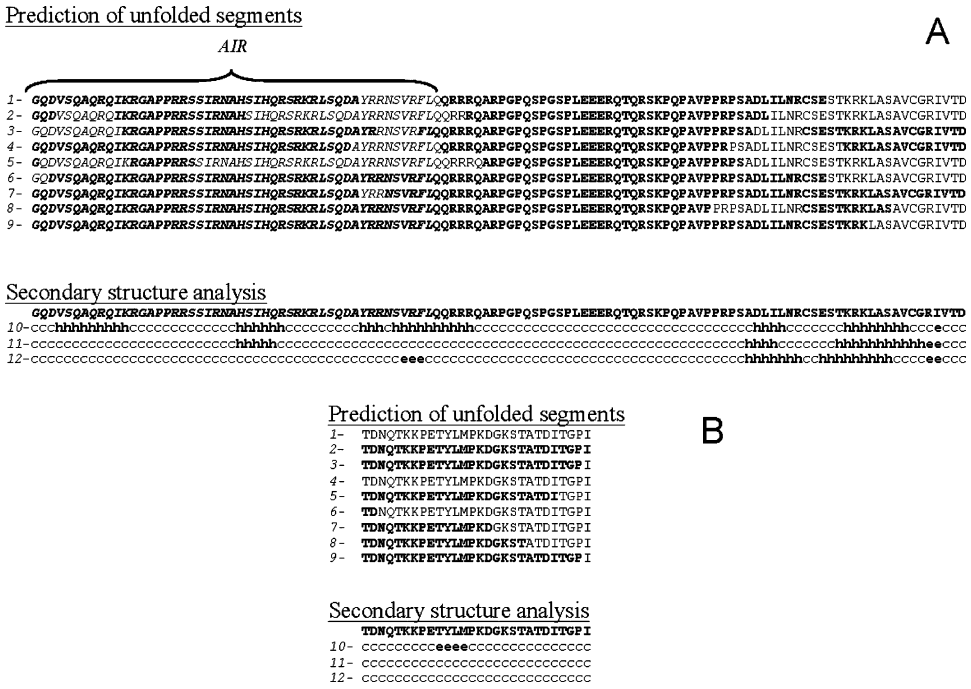

FIGURE 4: Prediction of unfolded segments and secondary structure analysis of the C-terminal region (A) and of the 28 residue-long linker connecting the PX domain to the tandem-SH3s/AIRregion (B). Segments predicted to be unfolded are in bold. c, coil; **h**, helix; **e**, extended. (1) Prelink (*38*); (2) DisEMBL, Loops/coils (*39*); (3) DisEMBL, Hot-loops; (4) DisEMBL, Remark-465; (5) Globplot (*40*); (6) PONDR (*41*, *42*); (7) RONN (*43*); (8) Foldindex (http://bip.weizmann.ac.il/fldbin/findex); (9) DISOPRED (*45*); (10) JPRED (*46*); (11) PSIPRED (*47*, *48*); (12) PHD (*49*).

seems to rule out any role in the preservation of the resting state.

In contrast, predictions regarding the AIR region are more variable, the region appearing to be more or less structured in 5 out of 9 analyses (lines 1−5 in Figure 4A). This is in agreement with the fact that it appears to be ordered and in interaction with the SH3 tandem in both crystal and NMR studies (*16*, *25*). Actually, the absence of a strong consensus toward a well-defined structure suggests that this segment is structured through its interaction with the two SH3 domains and that losing the interaction might cause the AIR region to lose its structure as well.

(ii) The 28 residue-long linker connecting the PX domain to the tandem-SH3s/AIR region does not appear to adopt a random coil configuration nor a compact conformation in the BUNCH models. This parallels the results of sequence analysis programs that do not give a clear and consistent view of the region, neither structured nor totally unfolded, beyond a large solvent accessibility (Figure 4B). A contribution of this linker to constraining the mutual arrangement of the structured domains cannot be ruled out.

(iii) The initial position of the PX domain and of the tandem SH3s/AIR domain directly derives from a combination of ab initio modeling (GASBOR model) and high-resolution crystal structures of the two domains. In this conformation, the two domains are weakly connected and a direct contact, highlighted in Figure 3C, can be observed, which involves the PX domain and a loop from the AIR sequence, protruding from the tandem-SH3s/AIR complex. Furthermore, the accessibility of the arginine residues from PX to membrane lipids appears hindered by the tandem SH3s/AIR domain and the intervening linker in most configurations. However, the mutual orientation of the structured domains is not uniquely defined by the SAXS data. Allowing for position refinement by the program BUNCH results in configurations in which the two domains are not in contact anymore. They remain in close vicinity, but the orientation of the PX domain appears to be hardly constrained as shown by the three models in Figure 3D in which the PX domain orientations, best visualized by the short N-terminal tail, are very different from one another as well as from the original one seen in Figure 3C. Our data are thus compatible with two classes of models according to whether the structured domains are in direct interaction or not. SAXS data cannot by themselves discriminate between the two possibilities and should be complemented by other approaches such as NMR using residual dipolar couplings determination (*51*, *52*) or mass spectrometry analysis of covalent cross-linking (*53*).

An intramolecular interaction of the PX domain seems necessary for the preservation of the resting state. Indeed, in the absence of stable contact with some part of the molecule, a well-defined position and orientation of the PX domain is difficult to conceive. It would most likely move fairly freely around the linker, thereby frequently exposing lipid binding arginine residues to the solvent, a situation difficult to reconcile with PX inhibition.

In a recent review, it has been proposed that the PX domain interacts with the whole tandem SH3s/AIR structured region rather than with the isolated $SH3_B$ domain (*4*). Our models with interacting structured domains (Figure 3C) provide an example of such an interaction between the loop in the C-terminal part of the AIR and the PX domain that could ensure PX inhibition, with a possible contribution from part of the linker connecting the PX to the tandem SH3 domains. Other interactions are certainly possible, which also make PX binding sites inaccessible to membrane lipids, but they all must exhibit a small buried interface imposed by

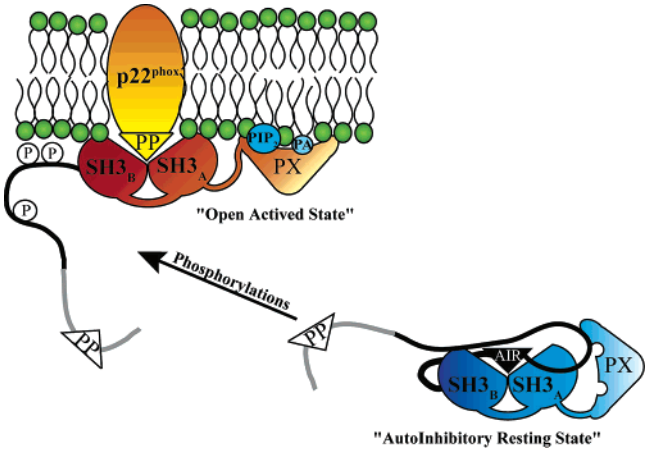

FIGURE 5: Proposed model for the autoinhibitory resting state of p47phox and phosphorylation-dependent association with lipids and p22phox. In the resting state, binding sites of PX and SH3 domains are hidden through intramolecular interactions. Phosphorylation of Ser 303, 304, and 328 disrupt these interactions, freeing both the PX and the tandem SH3s for interaction with lipids and p22phox, respectively. PP, PA, and PIP2 refer to the C-terminal polyproline region, phosphatidic acid, and phosphatidyl 3,4 inositol, respectively. The protein stretch displayed in black corresponds to the autoInhibitory region of p47phox.

the extended global conformation of p47phox as illustrated in the diagram shown in Figure 5. Such an interaction between PX domain and following domains of p47phox is supported by microcalorimetric titration experiments (*16*). These data show that the presence of the PX domain increases by a factor of 3 the affinity of the tandem SH3s for a peptide corresponding to the AIR sequence (residue 296−330) with respect to the isolated tandem-SH3s region. It suggests some contribution from PX through either direct contact with the AIR sequence or indirect stabilizing effect via interaction with the tandem of SH3 domains.

Phosphorylation of Ser 303, 304, and 328 is generally believed to alter the AIR conformation so as to destabilize its interaction with tandem SH3 domains, thereby making them free to interact with the proline-rich sequence of p22phox. We simply propose that another, direct or indirect, consequence of AIR conformational change would be to set the PX domain essentially free to move around the linker to $SH3_A$, thereby making its lipid binding sites available for interaction with phosphatidyl inositol lipids from the plasma membrane (see Figure 5). This hypothesis finds some support from data reported on a homologue of p47phox, NoxO1 (or p41), a cytosolic factor of Nox1, a homologue of the flavocytochrome b_{558} which is constitutively activated (*54*−*56*). In NoxO1, the PX domain has been shown to interact constitutively with phosphatidyl inositol lipids (*57*). In addition, the stimulus-independent superoxide production by Nox1 can be converted into a stimulus-dependent system when replacing NoxO1 by p47phox in a reconstituted whole cell system (*54*). Interestingly, in contrast to p47phox, NoxO1 does not contain an AIR sequence, an absence which correlates with a constitutive association to the membrane.

In conclusion, we have shown that p47phox adopts an extended conformation in the resting state. The two structured domains must be in close vicinity but can only be weakly connected, when at all in contact, their interacting surface area being small, while the C-terminal part, essentially unstructured, extends away from the structured domains. Work is under way, using complementary approaches to SAXS, to characterize further the interactions ensuring PX inhibition.

ACKNOWLEDGMENT

We are very grateful to Maxim Petoukhov for making the program Bunch available to us before its general distribution and for fruitful discussions regarding its use. We thank the technical staff from LURE-DCI. We thank M. C. Dagher for the kind gift of the p47phox containing expression vector.

REFERENCES

1. Vignais, P. V. (2002) The superoxide-generating NADPH oxidase: structural aspects and activation mechanism, *Cell. Mol. Life Sci. 59*, 1428−1459.
2. Babior, B. M. (2004) NADPH oxidase, *Curr. Opin. Immunol. 16*, 42−47.
3. Perisic, O., Wilson, M. I., Karathanassis, D., Bravo, J., Pacold, M. E., Ellson, C. D., Hawkins, P. T., Stephens, L., and Williams, R. L. (2004) The role of phosphoinositides and phosphorylation in regulation of NADPH oxidase, *Adv. Enzyme Regul. 44*, 279−298.
4. Groemping, Y., and Rittinger, K. (2005) Activation and assembly of the NADPH oxidase: a structural perspective, *Biochem. J. 386*, 401−416.
5. El Benna, J., Faust, R. P., Johnson, J. L., and Babior, B. M. (1996) Phosphorylation of the respiratory burst oxidase subunit p47phox as determined by two-dimensional phosphopeptide mapping. Phosphorylation by protein kinase C, protein kinase A, and a mitogen-activated protein kinase, *J. Biol. Chem. 271*, 6374−6378.
6. El Benna, J., Faust, L. P., and Babior, B. M. (1994) The phosphorylation of the respiratory burst oxidase component p47phox during neutrophil activation. Phosphorylation of sites recognized by protein kinase C and by proline-directed kinases, *J. Biol. Chem. 269*, 23431−23436.
7. Johnson, J. L., Park, J. W., Benna, J. E., Faust, L. P., Inanami, O., and Babior, B. M. (1998) Activation of p47(PHOX), a cytosolic subunit of the leukocyte NADPH oxidase. Phosphorylation of ser-359 or ser-370 precedes phosphorylation at other sites and is required for activity, *J. Biol. Chem. 273*, 35147−35152.
8. Inanami, O., Johnson, J. L., McAdara, J. K., El Benna, J., Faust, L. R., Newburger, P. E., and Babior, B. M. (1998) Activation of the leukocyte NADPH oxidase by phorbol ester requires the phosphorylation of p47PHOX on serine 303 or 304, *J. Biol. Chem. 273*, 9539−9543.
9. Faust, L. R., El Benna, J., Babior, B. M., and Chanock, S. J. (1995) The phosphorylation targets of p47phox, a subunit of the respiratory burst oxidase. Functions of the individual target serines as evaluated by site-directed mutagenesis, *J. Clin. Invest. 96*, 1499−1505.
10. Heyworth, P. G., Curnutte, J. T., Nauseef, W. M., Volpp, B. D., Pearson, D. W., Rosen, H., and Clark, R. A. (1991) Neutrophil nicotinamide adenine dinucleotide phosphate oxidase assembly. Translocation of p47-phox and p67-phox requires interaction between p47-phox and cytochrome b558, *J. Clin. Invest. 87*, 352−356.
11. Dusi, S., Donini, M., and Rossi, F. (1996) Mechanisms of NADPH oxidase activation: translocation of p40phox, Rac1 and Rac2 from the cytosol to the membranes in human neutrophils lacking p47phox or p67phox, *Biochem. J. 314*, 409−412.
12. Kanai, F., Liu, H., Field, S. J., Akbary, H., Matsuo, T., Brown, G. E., Cantley, L. C., and Yaffe, M. B. (2001) The PX domains of p47phox and p40phox bind to lipid products of PI(3)K, *Nat. Cell Biol. 3*, 675−678.
13. Karathanassis, D., Stahelin, R. V., Bravo, J., Perisic, O., Pacold, C. M., Cho, W., and Williams, R. L. (2002) Binding of the PX domain of p47(phox) to phosphatidylinositol 3,4-bisphosphate and phosphatidic acid is masked by an intramolecular interaction, *EMBO J. 21*, 5057−5068.
14. Sumimoto, H., Kage, Y., Nunoi, H., Sasaki, H., Nose, T., Fukumaki, Y., Ohno, M., Minakami, S., and Takeshige, K. (1994) Role of Src homology 3 domains in assembly and activation of the phagocyte NADPH oxidase, *Proc. Natl. Acad. Sci. U.S.A. 91*, 5345−5349.

15. Leto, T. L., Adams, A. G., and de Mendez, I. (1994) Assembly of the phagocyte NADPH oxidase: binding of Src homology 3 domains to proline-rich targets, *Proc. Natl. Acad. Sci. U.S.A. 91*, 10650−10654.
16. Groemping, Y., Lapouge, K., Smerdon, S. J., and Rittinger, K. (2003) Molecular basis of phosphorylation-induced activation of the NADPH oxidase, *Cell 113*, 343−355.
17. Ogura, K., Nobuhisa, I., Yuzawa, S., Takeya, R., Torikai, S., Saikawa, K., Sumimoto, H., and Inagaki, F. (2006) NMR Solution structure of the tandem Src homology 3 domains of p47phox complexed with a p22phox-derived proline-rich peptide, *J. Biol. Chem.. 281*, 3660−3668.
18. DeLeo, F. R., Nausseef, W. M., Jesaitis, A. J., Burritt, J. B., Clark, R. A., and Quinn, M. T. (1995) A domain of p47phox that interacts with human neutrophil flavocytochrome b_{558}, *J. Biol. Chem. 270*, 26246−26251.
19. DeLeo, F. R., Yu, L., Burritt, J. B., Loetterle, L. R., Bond, C. W., Jesaitis, A. J., and Quinn, M. T. (1995) Mapping sites of interaction of p47-*phox* and flavocytochrome b with random-sequence peptide phage display libraries, *Proc. Natl. Acad. Sci. U.S.A. 92*, 7110−7114.
20. Ago, T., Nunoi, H., Ito, T., and Sumimoto, H. (1999) Mechanism for phosphorylation-induced activation of the phagocyte NADPH oxidase protein p47(phox). Triple replacement of serines 303, 304, and 328 with aspartates disrupts the SH3 domain-mediated intramolecular interaction in p47(phox), thereby activating the oxidase, *J. Biol. Chem. 274*, 33644−33653.
21. Ago, T., Kuribayashi, F., Hiroaki, H., Takeya, R., Ito, T., Kohda, D., and Sumimoto, H. (2003) Phosphorylation of p47phox directs phox homology domain from SH3 domain toward phosphoinositides, leading to phagocyte NADPH oxidase activation, *Proc. Natl. Acad. Sci. U.S.A. 100*, 4474−4479.
22. Shiose, A., and Sumimoto, H. (2000) Arachidonic acid and phosphorylation synergistically induce a conformational change of p47phox to activate the phagocyte NADPH oxidase, *J. Biol. Chem. 275*, 13793−13801.
23. Hiroaki, H., Ago, T., Ito, T., Sumimoto, H., and Kohda, D. (2001) Solution structure of the PX domain, a target of the SH3 domain, *Nat. Struct. Biol. 8*, 526−530.
24. de Mendez, I., Homayounpour, N., and Leto, T. L. (1997) Specificity of p47phox SH3 domain interactions in NADPH oxidase assembly and activation, *Mol. Cell. Biol. 17*, 2177−2185.
25. Yuzawa, S., Suzuki, N. N., Fujioka, Y., Ogura, K., Sumimoto, H., and Inagaki, F. (2004) A molecular mechanism for autoinhibition of the tandem SH3 domains of p47phox, the regulatory subunit of the phagocyte NADPH oxidase, *Genes Cells 9*, 443−456.
26. Yuzawa, S., Ogura, K., Horiuchi, M., Suzuki, N. N., Fujioka, Y., Kataoka, M., Sumimoto, H., and Inagaki, F. (2004) Solution structure of the tandem Src homology 3 domains of p47phox in an autoinhibited form, *J. Biol. Chem. 279*, 29752−29760.
27. Dubuisson, J. M., Decamps, T., and Vachette, P. (1997) Improved signal-to-background ratio in small-angle X-ray scattering experiments with synchrotron radiation using an evacuated cell for solutions, *J. Appl. Crystallogr. 30*, 49−54.
28. Mangenot, S., Leforestier, A., Vachette, P., Durand, D., and Livolant, F. (2002) Salt-induced conformation and interaction changes of nucleosome core particles, *Biophys. J. 82*, 345−356.
29. Guinier, A., and Fournet, G. (1955) *Small Angle Scattering of X-rays*, Wiley, New York.
30. Svergun, D. I. (1992) Determination of the regularization parameter in indirect-transform methods using perceptual criteria, *J. Appl. Crystallogr. 25*, 495−503.
31. Svergun, D. I. (1999) Restoring low resolution structure of biological macromolecules from solution scattering using simulated annealing, *Biophys. J. 76*, 2879−2886.
32. Svergun, D. I., Petoukhov, M. V., and Koch, M. H. (2001) Determination of domain structure of proteins from X-ray solution scattering, *Biophys. J. 80*, 2946−2953.
33. Kozin, M. B., and Svergun, D. I. (2001) Automated matching of high- and low-resolution structural models, *J. Appl. Crystallogr. 34*, 33−41.
34. Petoukhov, M. V., and Svergun, D. I. (2005) Global rigid body modeling of macromolecular complexes against small-angle scattering data, *Biophys. J. 89*, 1237−1250..
35. Svergun, D. I., Barberato, C., and Koch, M. H. (1995) CRYSOL−a program to evaluate X-ray solution scattering of biological macromolecules from atomic coordinates, *J. Appl. Crystallogr. 28*, 768−773.
36. Pérez, J., Vachette, P., Russo, D., Desmadril, M., and Durand, D. (2001) Heat-induced unfolding of neocarzinostatin, a small all-beta protein investigated by small-angle X-ray scattering, *J. Mol. Biol. 308*, 721−743.
37. Rowe, G., and Lopez Pineiro, A. (1990) Influence of the solvent on the conformational-dependent properties of random-coil polypeptides. I. The mean-square of the end-to-end distance and of the dipole moment, *Biophys. Chem. 36*, 57−64.
38. Coeytaux, K., and Poupon, A. (2005) Prediction of unfolded segments in a protein sequence based on amino acid composition, *Bioinformatics 18*, 18.
39. Linding, R., Jensen, L. J., Diella, F., Bork, P., Gibson, T. J., and Russell, R. B. (2003) Protein disorder prediction: implications for structural proteomics, *Structure (London) 11*, 1453−1459.
40. Linding, R., Russell, R. B., Neduva, V., and Gibson, T. J. (2003) GlobPlot: exploring protein sequences for globularity and disorder, *Nucleic Acids Res. 31*, 3701−3708.
41. Li, X., Romero, P., Rani, M., Dunker, A. K., and Obradovic, Z. (1999) Predicting protein disorder for N-, C-, and internal regions, *Genome Inf. 10*, 30−40.
42. Romero, P., Obradovic, Z., Li, X., Garner, E., Brown, C., and Dunker, A. K. (2001) Sequence complexity of disordered protein, *Proteins: Struct., Funct., Genet. 42*, 38−48.
43. Thomson, R., and Esnouf, R. (2004) Prediction of natively disordered regions in proteins using a bio-basis function neural network, in *Lecture Notes in Computer Science* (Yang, Z. R., Yin, H., and Everson, R., Eds.) Vol. 3177, pp 108−116, Springer, Berlin and Heidelberg.
44. Uversky, V. N., Gillespie, J. R., and Fink, A. L. (2000) Why are "natively unfolded" proteins unstructured under physiologic conditions? *Proteins 41*, 415−427.
45. Ward, J. J., Sodhi, J. S., McGuffin, L. J., Buxton, B. F., and Jones, D. T. (2004) Prediction and functional analysis of native disorder in proteins from the three kingdoms of life, *J. Mol. Biol. 337*, 635−645.
46. Cuff, J. A., and Barton, G. J. (2000) Application of multiple sequence alignment profiles to improve protein secondary structure prediction, *Proteins 40*, 502−511.
47. McGuffin, L. J., Bryson, K., and Jones, D. T. (2000) The PSIPRED protein structure prediction server, *Bioinformatics 16*, 404−405.
48. Jones, D. T. (1999) Protein secondary structure prediction based on position-specific scoring matrices, *J. Mol. Biol. 292*, 195−202.
49. Rost, B., Yachdav, G., and Liu, J. (2004) The PredictProtein server, *Nucleic Acids Res. 32*, W321−326.
50. Kami, K., Takeya, R., Sumimoto, H., and Kohda, D. (2002) Diverse recognition of non-PxxP peptide ligands by the SH3 domains from p67(phox), Grb2 and Pex13p, *EMBO J. 21*, 4268−4276.
51. Gabel, F., Simon, B., and Sattler, M. (2006) A target function for quaternary structural refinement from small angle scattering and NMR orientational restraints, *Eur. Biophys. J.* 1−15.
52. Grishaev, A., Wu, J., Trewhella, J., and Bax, A. (2005) Refinement of multidomain protein structures by combination of solution small-angle X-ray scattering and NMR data, *J. Am. Chem. Soc. 127*, 16621−16628.
53. Back, J. W., de Jong, L., Muijsers, A. O., and de Koster, C. G. (2003) Chemical cross-linking and mass spectrometry for protein structural modeling, *J. Mol. Biol. 331*, 303−313.
54. Banfi, B., Clark, R. A., Steger, K., and Krause, K. H. (2003) Two novel proteins activate superoxide generation by the NADPH oxidase NOX1, *J. Biol. Chem. 278*, 3510−3513.
55. Geiszt, M., Lekstrom, K., Witta, J., and Leto, T. L. (2003) Proteins homologous to p47phox and p67phox support superoxide production by NAD(P)H oxidase 1 in colon epithelial cells, *J. Biol. Chem. 278*, 20006−20012.
56. Suh, Y. A., Arnold, R. S., Lassegue, B., Shi, J., Xu, X., Sorescu, D., Chung, A. B., Griendling, K. K., and Lambeth, J. D. (1999) Cell transformation by the superoxide-generating oxidase Mox1, *Nature 401*, 79−82.
57. Cheng, G., and Lambeth, J. D. (2004) NOXO1, regulation of lipid binding, localization, and activation of Nox1 by the Phox homology (PX) domain, *J. Biol. Chem. 279*, 4737−4742.
58. Grizot, S., Grandvaux, N., Fieschi, F., Faure, J., Massenet, C., Andrieu, J. P., Fuchs, A., Vignais, P. V., Timmins, P. A., Dagher, M. C., and Pebay-Peyroula, E. (2001) Small angle neutron scattering and gel filtration analyses of neutrophil NADPH oxidase cytosolic factors highlight the role of the C-terminal end of $p47^{phox}$ in the association with $p40^{phox}$ *Biochemistry 40*, 3127−3133.

59. Ito, T., Nakamura, R., Sumimoto, H., Takeshige, K., and Sakaki, Y. (1996) An SH3 domain-mediated interaction between the phagocyte NADPH oxidase factors p40phox and p47phox, *FEBS Lett. 385*, 229−232.
60. Fuchs, A., Dagher, M. C., Faure, J., and Vignais, P. V. (1996) Topological organization of the cytosolic activating complex of the superoxide-generating NADPH-oxidase. Pinpointing the sites of interaction between p47phoz, p67phox and p40phox using the two-hybrid system, *Biochim. Biophys. Acta 1312*, 39−47.
61. Fuchs, A., Dagher, M. C., and Vignais, P. V. (1995) Mapping the domains of interaction of p40phox with both p47phox and p67phox of the neutrophil oxidase complex using the two-hybrid system, *J. Biol. Chem. 270*, 5695−5697.
62. Sumimoto, H., Hata, K., Mizuki, K., Ito, T., Kage, Y., Sakaki, Y., Fukumaki, Y., Nakamura, M., and Takeshige, K. (1996) Assembly and activation of the phagocyte NADPH oxidase. Specific interaction of the N-terminal Src homology 3 domain of p47phox with p22phox is required for activation of the NADPH oxidase, *J. Biol. Chem. 271*, 22152−22158.
63. Ago, T., Takeya, R., Hiroaki, H., Kuribayashi, F., Ito, T., Kohda, D., and Sumimoto, H. (2001) The PX domain as a novel phosphoinositide-binding module, *Biochem. Biophys. Res. Commun. 287*, 733−738.
64. Lapouge, K., Smith, S. J., Groemping, Y., and Rittinger, K. (2002) Architecture of the p40-p47-p67phox complex in the resting state of the NADPH oxidase. A central role for p67phox, *J. Biol. Chem. 277*, 10121−10128.
65. Nauseef, W. M. (2004) Assembly of the phagocyte NADPH oxidase, *Histochem. Cell Biol. 122*, 277−291.

BI060274K